Supporting Information for

UV-Resonant Al Nanocrystals: Synthesis, Silica Coating, and Broadband Photothermal Response

David Renard, [†,‡] *Shu Tian,* [†,‡] *Minhan Lou,* [‡,∥] *Oara Neumann,* [‡,∥] *Jian Yang,* [‡,⊥] *Aaron Bayles,* [†,‡] *David Solti,* [†,‡] *Peter Nordlander,* [‡,∥,⊥] *and Naomi J. Halas** [†,‡,∥,⊥]

[†]Department of Chemistry, [‡]Laboratory for Nanophotonics, [∥]Department of Electrical and Computer Engineering, [⊥]Department of Physics and Astronomy, Rice University, 6100 Main Street, Houston, Texas 77005, United States.

Materials. Trioctylphosphine (97%), N,N-dimethylethylamine alane (0.5M in toluene), titanium (IV) isopropoxide (99.999%), anhydrous toluene, dibutylphosphate (97%), anhydrous cyclohexane, isopropanol (ACS grade), (3-aminopropyl)triethoxysilane (99%), and NH_4OH (28-30% in H_2O) were obtained from Millipore Sigma and used without further purification. Tetraethyl orthosilicate (98%) was obtained from Acros Organics and used as received. 10K MW PEG-Silane was obtained from Nanocs INC and stored at 4C in a desiccator.

Characterization. TEM imaging was performed using a 1230 JEOL High Contrast TEM operating at 80 kV. High resolution TEM imaging was performed using a 2100F JEOL TEM operating at 200 kV. UV-vis spectra were taken using a Cary 5000 UV−vis spectrometer and quartz cuvettes. To obtain increasingly concentrated Al NC samples for UV-Vis, a high concentration sample obtained after washing, is sequentially diluted to avoid issues of induced aggregation and to maintain the same sample size distribution between the varyingly concentrated samples.

Synthesis of Al NCs. Small Al NCs were synthesized using a modified approach to previous publications.[1-3] Briefly, 24 mL of degassed trioctylphosphine was heated to 60C with vigorous stirring in an argon purged Schlenk flask using an oil bath. Next, 6 mL of N,N-dimethylethylamine alane (0.5M in toluene) was added *via* syringe and allowed to stir for 5 minutes. Then, 1.5 mL of Titanium(IV) isopropoxide (50 mM in toluene) was added *via* syringe to catalyze the decomposition of alane into metallic Al. The reaction becomes a dark, translucent brown color upon addition of Ti(IV) that gradually changes to an opaque black, indicating the formation of small Al NCs. The reaction was stirred for 4 hours at 60 °C under argon flow, then 10 mL of dibutyl phosphate (50 mM in cyclohexane) was added to cap the particle surface. The flask was

then opened to air forming a 3-5 nm, self-limiting, amorphous Al_2O_3 layer at the particle surface. This oxide layer prevents further oxidation of the underlying Al core by air however care must be taken to avoid exposure to water as the particles are highly susceptible to oxidation by water. The nanoparticles were collected *via* multiple rounds of centrifugation and resuspension in isopropanol. To remove aggregates or large particles formed during synthesis, the sample is centrifuged up to 4 times at 15,000x g, keeping the supernatant each time and discarding the pellet. In this way, the sample size distribution is narrowed and the UV-resonant response sharpened.

SiO_2 Functionalization. SiO_2 functionalization was accomplished using a modified version of the Stöber process.[4] The following procedure yields a 20 nm layer of SiO_2 on the Al NCs. To tune the SiO_2 thickness, the amounts of TEOS/APTES can be tuned according to Figure S3. 50 mL of 90% ethanol was stirred rapidly at room temperature. Then 0.5 mL of Al NCs in isopropanol were added, yielding a pale, yellow solution. 0.5 mL of aqueous NH_4OH was added to the flask and was quickly followed by 20 µL of 10% TEOS solution in ethanol and 5 µL of 10% APTES solution in 100% ethanol. It is important that these two solutions are made fresh directly prior to the synthesis. Then the flask was capped and stirred at room temperature for 1 hour at 300 rpm. Then the flask was transferred to a refrigerator and stirred at 300 rpm for 24 hours at 4 °C. The samples were then allowed to sit, undisturbed for 2h at 4 C to allow any aggregated particles to settle to the bottom of the flask. The samples were carefully decanted into dialysis bags and dialyzed in 100% ethanol overnight at room temperature to remove excess reagents. The samples were then collected and concentrated *via* 3 cycles of centrifugation and resuspension in ethanol. PEG functionalization on the surface of the particles was accomplished by making a stock solution of 10k MW PEG-Silane in water (1mg/mL) and stirring the concentrated Al@SiO_2 samples in the PEGylation solution for 4h at RT. Excess reagents were removed *via* centrifugation and resuspension in ethanol.

Lumerical FDTD simulations. The optical properties of one single Al sphere of different sizes and one silica sphere in air were both performed by the finite-difference-time-domain (FDTD) method (Lumerical solutions 2019b). The absorption and scattering cross-section spectra of a single nanoparticle in environment with refractive index of 1.33 were calculated by the broad-band multi-frequency total-field-scattered-field (TFSF) approach with normal incident light. The absorption cross sections were calculated by power flux of total field through a closed surface. The scattering cross sections were calculated by power flux of scattered field through a closed surface.

$\sigma_{absorption,ensemble}(\omega)$ and $\sigma_{scattering,ensemble}(\omega)$, the absorption and scattering cross-section spectra respectively of a nanoparticle ensemble with varying sizes, were calculated as weighted cross-sections with respect to the size distribution

$$\sigma_{absorption,ensemble}(\omega) = \sum_{D=10\,nm}^{50\,nm} \sigma_{absorption}(\omega, D) \times P(D)$$

$$\sigma_{scattering,ensemble}(\omega) = \sum_{D=10\,nm}^{50\,nm} \sigma_{scattering}(\omega, D) \times P(D)$$

Where $\sigma_{absorption}(\omega, D)$ and $\sigma_{scattering}(\omega, D)$ were the absorption and scattering cross section spectra of the nanoparticle with size D respectively, $P(D)$ is the occurrence probability of

size D and ω is the angular frequency. The size values used in the summation were from 10 nm to 50 nm with 2.5 nm step. The mesh size of the particle was set to be the smaller value between 1/40 of the particle size and 0.5 nm.

Palik data,[5] and low loss single-crystalline data[6] were used as Al permittivity for comparison. The size corrected Palik dielectric constants were set as

Spherical Al particle with size D and 3 nm oxide layer was constructed by an Al sphere with dimeter $\mathrm{D} - 6\ \mathrm{nm}$ inside an Al_2O_3 sphere with dimeter D. The overlapping part were Al and the remaining part were Al_2O_3.

The truncated octahedron (TO) size was defined as the edge length of corresponding un-truncated octahedron. The unrounded TO was constructed by Planar Solid structure with corresponding vertex coordinates. All the edges and vertexes of truncated octahedron (TO) were achieved by extruding the facets of unrounded BC with the distance of rounding radius ($\mathrm{r_{round}}$) and filled gaps with spheres and cylinders of radius $\mathrm{r_{round}}$. All the simulated TOs with varying sizes had 5 nm rounding radius. A rounded TO with size of $\mathrm{D_{rounded}}$ and rounding radius $\mathrm{r_{round}}$ is built by adding above mentioned rounding layer with thickness $\mathrm{r_{round}}$ to an unrounded TO with size of $\mathrm{D_{rounded}} - 2\mathrm{r_{round}}$. The Al_2O_3 oxide layer is addition rounding layer of thickness of 3 nm. For example, a 20 nm oxidized Al TO with outer rounding radius of 5 nm and oxide layer thickness of 3 nm was constructed as a 10 nm unrounded Al TO, 2 nm thick Al rounding layer and additional 3 nm Al_2O_3 rounding layer.

Right bipyramids (RB) were twined right pyramids with regular triangle bases and right triangle lateral faces. Rounded oxidized Al RB were constructed in the same way mentioned above. All the simulated RBs had inner rounding radius (for inner Al) of the smaller value between 5 nm and 1/3 of the inner Al size. For example, a 15 nm RB with 3 nm oxide layer was constructed as a 3 nm unrounded Al RB, 3 nm Al rounding layer and additional 3 nm Al_2O_3 rounding layer. A 30 nm RB with 3 nm oxide layer was constructed as a 14 nm unrounded Al RB, 5 nm Al rounding layer and additional 3 nm Al_2O_3 rounding layer.

Since the SiO_2 coating looks spherical in the TEM, adding the 20 nm SiO_2 coating layer to a particle with size $\mathrm{D_{rounded}}$ was modeled as putting the particle inside a SiO_2 sphere with diameter $\mathrm{D_{rounded}} + 40\ \mathrm{nm}$.

Monte-Carlo simulations. The Monte-Carlo approach was used to calculate the transmission of light from a $1\mathrm{cm} \times 1\mathrm{cm} \times 1\mathrm{cm}$ box containing randomly distributed Au, Ag, Al, or CB nanoparticles in a solution. The Monte-Carlo simulation code was custom written in C language. The refractive index for solution was set as 1.33 and the initial position of injected photon was placed on the top solution/air interface with velocity normal to interface. At certain light wavelength, the photon transport distance x between two collision event is a random variable following the probability density function of $\alpha_{ext} \cdot e^{\alpha_{ext} \cdot x}$ where α_{ext} is the ensemble extinction coefficient.

$$\alpha_{ext} = \alpha_{scattering} + \alpha_{absorption}$$

$$\alpha_{scattering} = \sigma_{scattering,ensemble} \times n$$

$$\alpha_{absorption} = \sigma_{absorption,ensemble} \times n$$

where $\alpha_{scattering}$ is the ensemble scattering coefficient, $\alpha_{absorption}$ is the ensemble absorption coefficient, $\sigma_{absorption,ensemble}$ is the ensemble absorption cross-section, $\sigma_{scattering,ensemble}$ the ensemble scattering cross-section and n is particle number in a unit volume.

When a collision event happens, $\alpha_{absorption}/(\alpha_{absorption} + \alpha_{scattering})$ portion of photon power (initially set as 1) was absorbed and the photon with remaining power was scattered into new direction following unpolarized dipole far-field scattering profile. The transport of a single photon continued until the photon power was lower than a threshold level (considered totally absorbed) or escaped from the catalyst box. Then the remining photon power of the escaped photon from the bottom surface is added to the transmitted power. Millions of photons are injected in the box and the final transmission (T) is the total transmitted power of total photons divided by the total photon number.

Water stability experiments.

Water stability experiments were performed by dispersing 100 μL of either Al@SiO_2 or bare Al NCs in 1mL of ultrapure Millipore water in a sealed sample tube. Bare Al NCs used in this study were uncapped, as the common capping agents employed for Al NCs (dibutylphosphate or oleic acid) render them hydrophobic and induce irreversible aggregation in aqueous environment. Periodic TEM samples were made by dropcasting 10 mL on carbon coated TEM grids and allowing them to dry completely. For the 60 °C water stability testing, the aqueous samples were immersed in a temperature-controlled oil bath for the duration of the experiment. Care must be taken to ensure a tight seal on the sample tubes to prevent evaporative losses.

Photothermal measurements.

Photothermal measurements were done using a set-up comprised of 4 different components to simultaneously illuminate the sample, measure mass changes, and measure both surface and bulk temperature changes. Samples of Al@SiO_2 were dispersed in 1 mL of water and placed within a 1 x 1 x 1 cm^3 cuvette. The sample was positioned on a Sartorius Cubis analytical balance to measure changes in mass during illumination. Monochromatic light from a tunable Ti:sapphire laser (Coherent, Chameleon Ultra II, 150 fs, 80 MHz, 680−1080 nm, bandwidth ~10 nm) equipped with a second harmonic generator (Angewandte Physik und Elektronik GmbH, output wavelength 350−530 nm) was used to illuminate the sample, incident on the top surface of the liquid with a 5 mm spot size. A thermal camera (FLIR A65) was focused on the sample surface and used to track surface temperature changes of the liquid. A thin temperature probe was immersed in the bottom corner of the cuvette and attached to an Omega HH309A Four-Channel Data Logger as a measurement of the bulk temperature change within the cuvette.

Supplemental Figures

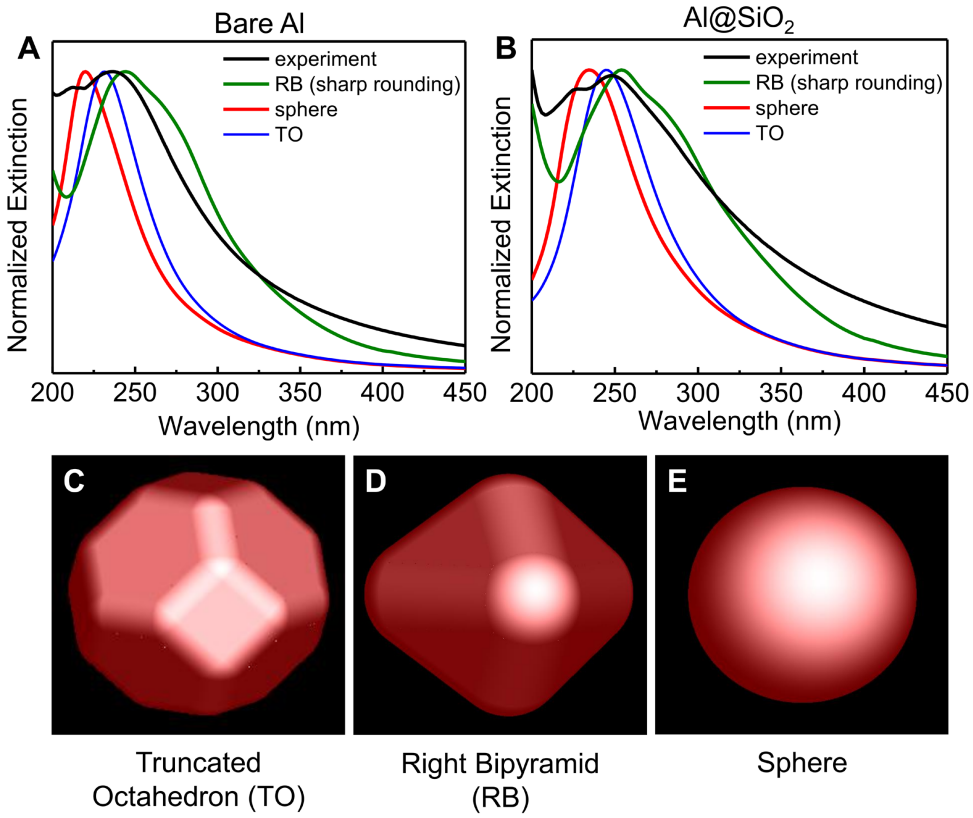

Figure S1. Simulated extinction spectra of Al NCs and Al@SiO_2 NCs of varying shape. Simulated extinction spectra of Al NCs (A) or Al@SiO_2 NCs (B) with either a truncated octahedron, right bipyramid, or sphere shape compared to experiment. In the case of SiO_2 coated NCs, the interior core is of varying shape with a spherical shell of SiO_2. Visual representations of the shaped used for simulation (C-E).

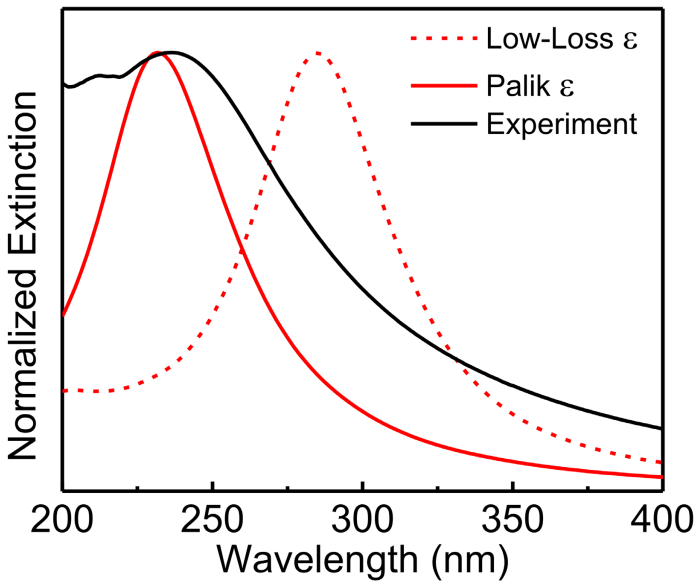

Figure S2. Simulated extinction of small Al NCs compared with experiment showing the influence of permittivity data on the resonance position compared to experiment. Palik and low-low data from refs 5 and 6, respectively.

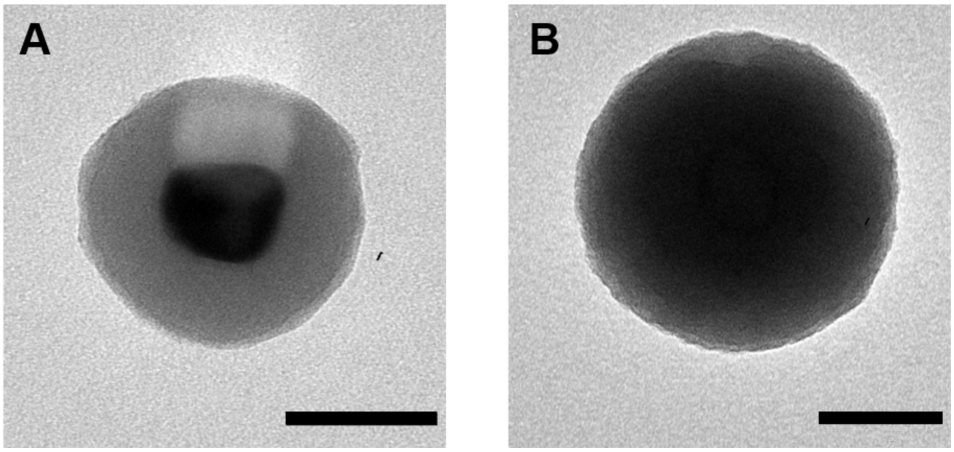

Figure S3. Representative brightfield TEM images of two different single Al@SiO_2 NCs highlighting the varying degree of diffraction contrast based on particle orientation. (A) Al core is oriented along the zone axis resulting in high degree of diffraction contrast between the crystalline Al core and the amorphous SiO_2 shell. (B) Al core is oriented off the zone axis, resulting in less diffraction contrast and less definition between the crystalline core and amorphous shell. Scale bars are 50 nm.

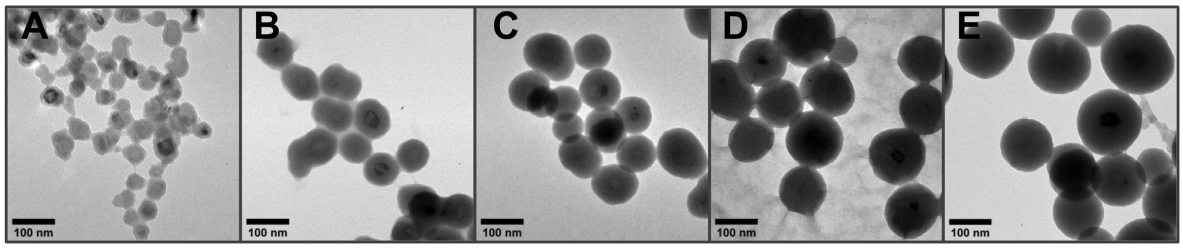

F

5 nm → 50 nm

Increasing TEOS and APTES concentration

Decreasing Al NCs concentration

G	**24 h reaction in refrigerator**				
EtOH	45 mL				
H_2O	5 mL				
NH_4OH	0.5 mL				
Al	0.5 mL	0.5 mL	0.5 mL	0.2 mL	0.5 mL
10% TEOS/EtOH	10 µL	20 µL	50 µL	50 µL	50 µL
10% APTES/EtOH	5 µL	5 µL	10 µL	10 µL	40 µL
SiO_2 Thickness	5 nm	20 nm	30 nm	40 nm	50 nm

Figure S4. Tuning of SiO_2 shell thickness. TEM images of the variable SiO_2 shell thickness of ~5 nm to ~50 nm (A-E) and the general methods for tuning the shell thickness– increasing TEOS/APTES concentration or decreasing Al NC concentration (F). Table summarizing the general ratios used in tuning the shell thickness (G). These values were determined for the specific concentration of Al NCs used in experiments and were adjusted accordingly to particle concentration for other samples.

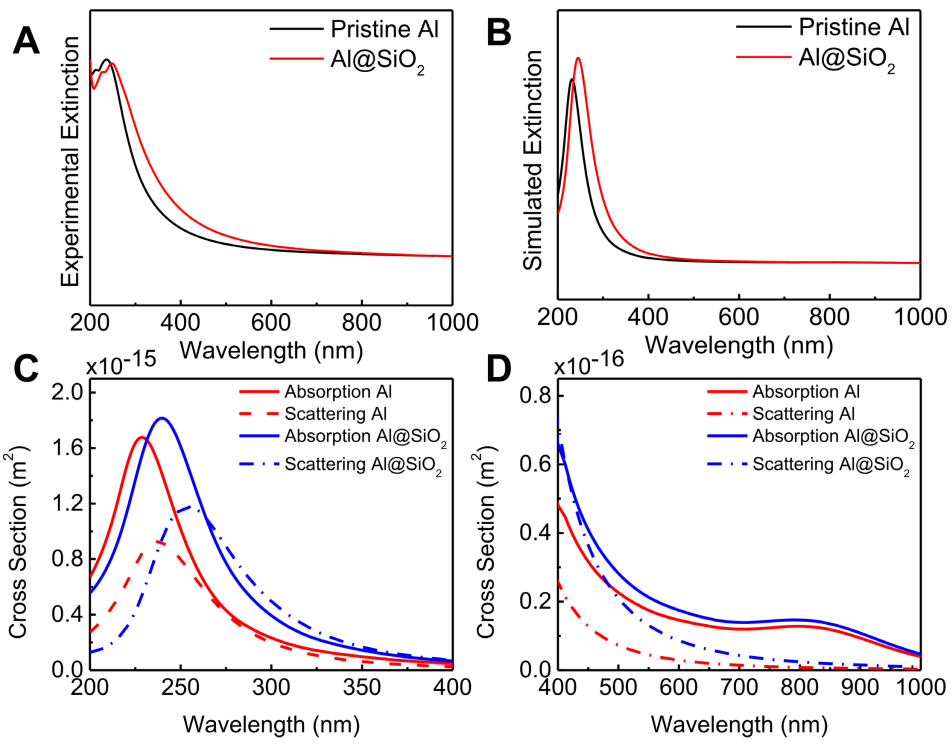

Figure S5. Optical properties of Al NCs and Al@SiO_2 NCs. (A) Experimental extinction spectra of pristine and 20 nm SiO_2 coated Al NCs and (B) corresponding simulated extinction spectra. (C) Simulated absorption (solid) and scattering (dashed) cross sections for bare (red) and 20 nm SiO_2 coated (blue) Al NCs dispersed in isopropanol. (A) Shows the UV region where the plasmon resonance lies and (B) shows the visible region where the absorption dominates. (B), (C), and (D) are size-weighted spectra based on experiment particle size distribution.

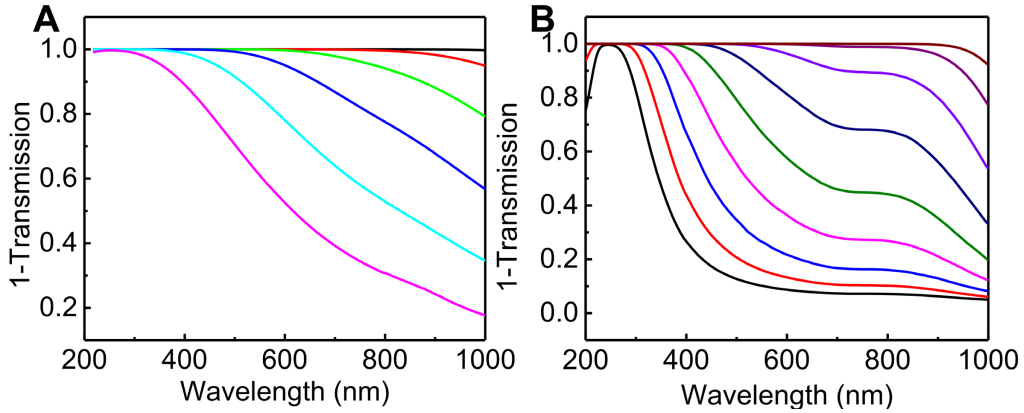

Figure S6. Experimental and Monte-Carlo simulations of increasingly concentrated Al@SiO_2. Experimental transmission spectrum of Al@SiO_2 NCs with increasing concentration (A) and corresponding Monte-Carlo simulations (B) showing a similar trend of decreasing transmission

with increasing concentration. The SiO_2 shell thickness was 20 nm in both experiment and simulation.

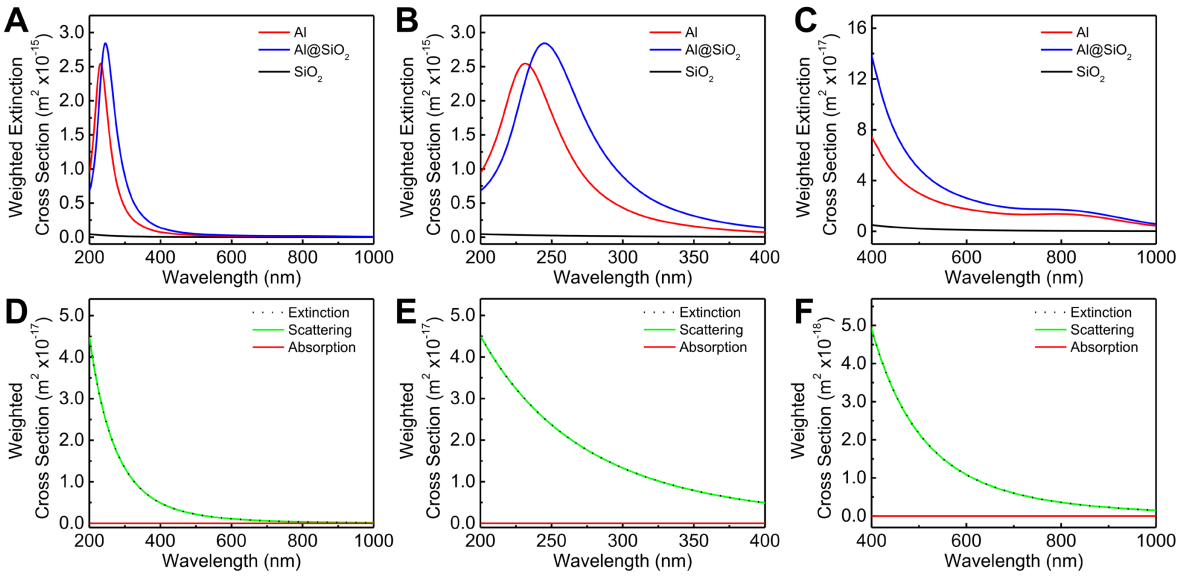

Figure S7. Extinction cross sections of Al, Al@SiO_2 and pure SiO_2 spheres for the full spectrum (A), UV (B), and visible (C) regions highlighting the importance of the Al core in the optical absorption. Optical cross sections of pure SiO_2 spheres for the full spectrum (D), UV (E), and visible (C), regions showing the purely scattering character of SiO_2. All spectra are weighted according to the experimentally determined size range.

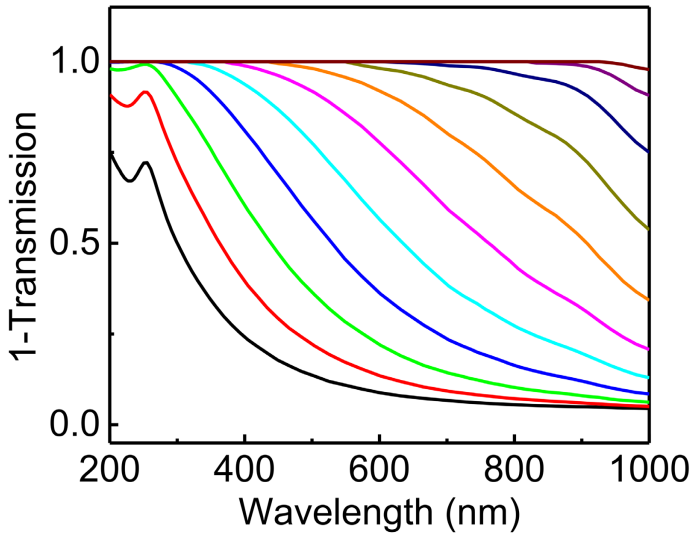

Figure S8. Monte-Carlo simulations of increasingly concentrated Al@SiO_2 with a shell thickness of 45 nm. A 3 nm Al_2O_3 layer separates the Al core from the SiO_2 shell. Particle concentration ranges from $1.25x10^{10}$ to $1.28x10^{12}$ NPs/cm^3.

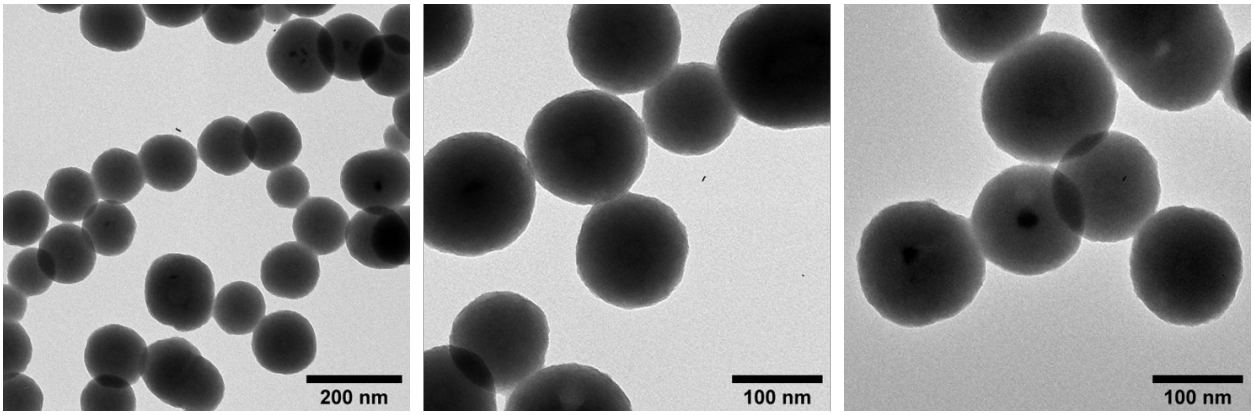

Figure S9. Additional TEM images of the as-synthesized Al@SiO_2 with a shell thickness of 45 nm functionalized with PEG-Silane (10k MW).

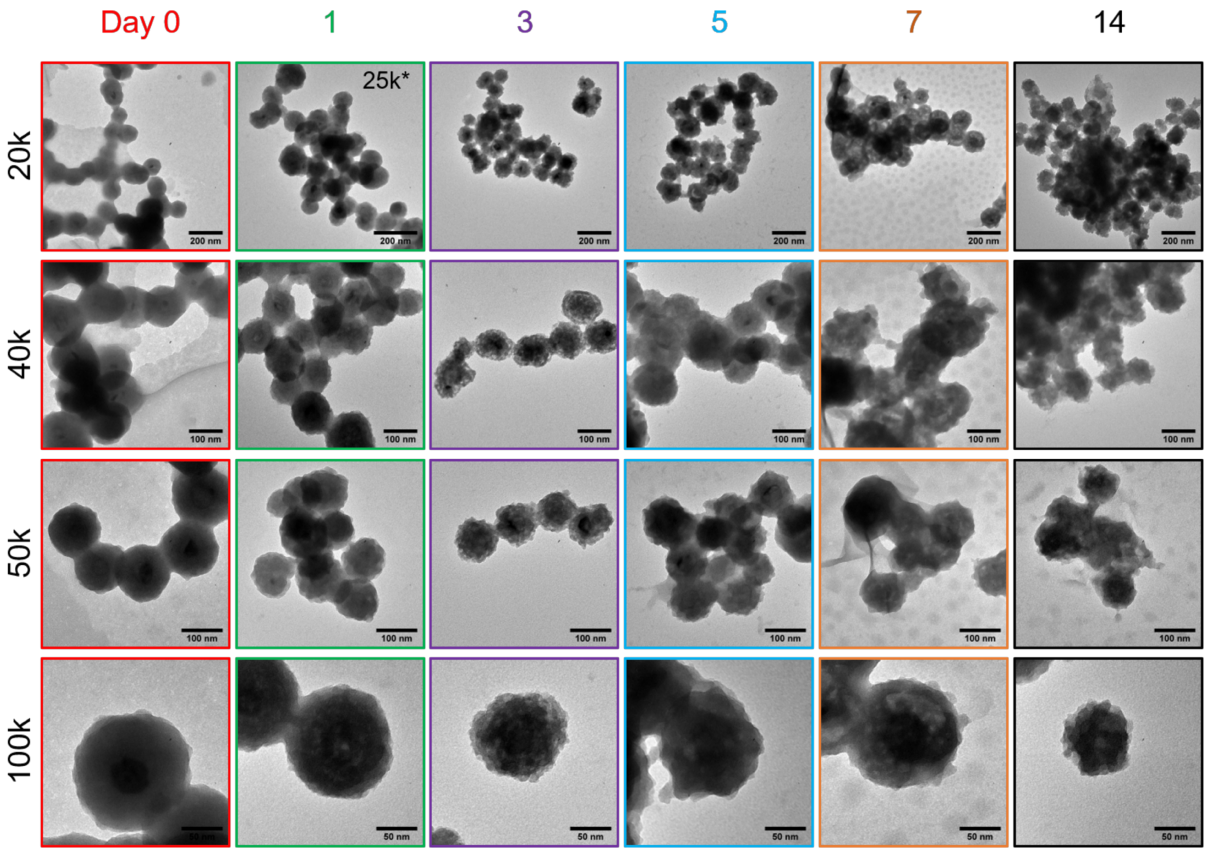

Figure S10. Additional TEM images of Al@SiO_2 dispersed in water over the course of 2 weeks at 60 °C. TEM magnification increases down a column and days in water increases across a row. Shell thickness ~45 nm.

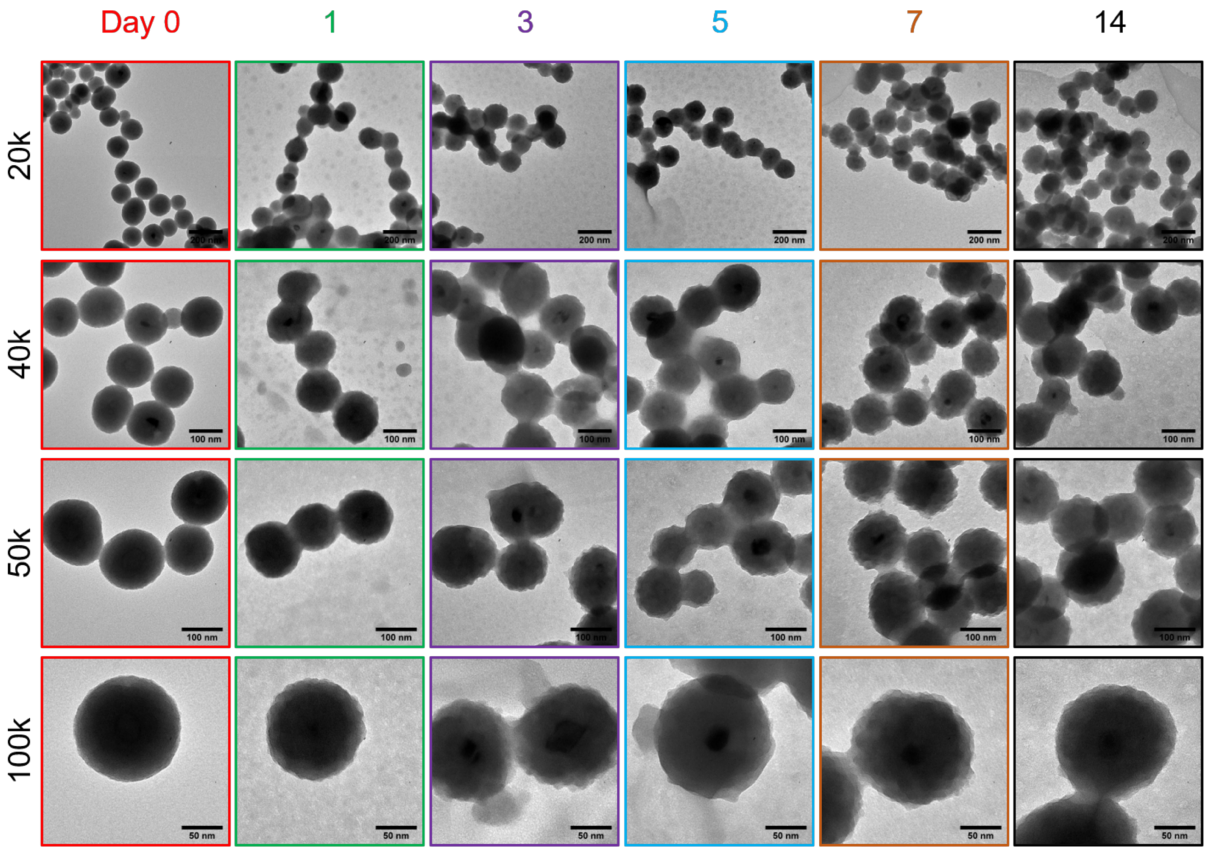

Figure S11. Additional TEM images of Al@SiO_2 dispersed in water over the course of 2 weeks at room temperature. TEM magnification increases down a column and days in water increases across a row. Shell thickness ~45 nm.

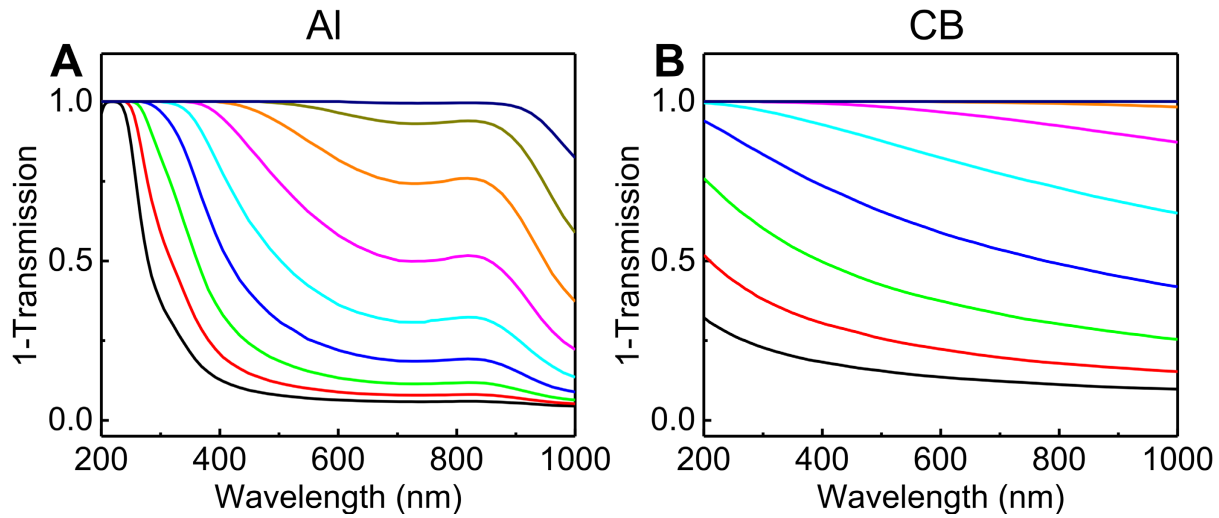

Figure S12. Monte-Carlo simulations of the transmission spectrum of increasingly concentrated 20 nm Al (A) or 20 nm carbon black (B) nanoparticles. For the Al case, the particle has a 3 nm Al_2O_3 shell. Particle concentration ranges from $2.0x10^{11}$ to $5.12x10^{13}$ NPs/mL in both cases.

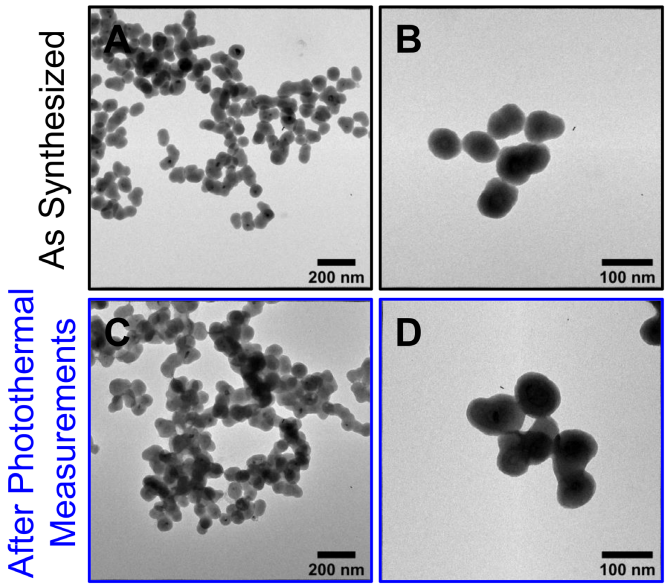

Figure S13. TEM images of Al@SiO_2 before (A,B) and after (C,D) multiple cycles of laser-induced photothermal heating in water. Shell thickness ~20 nm.

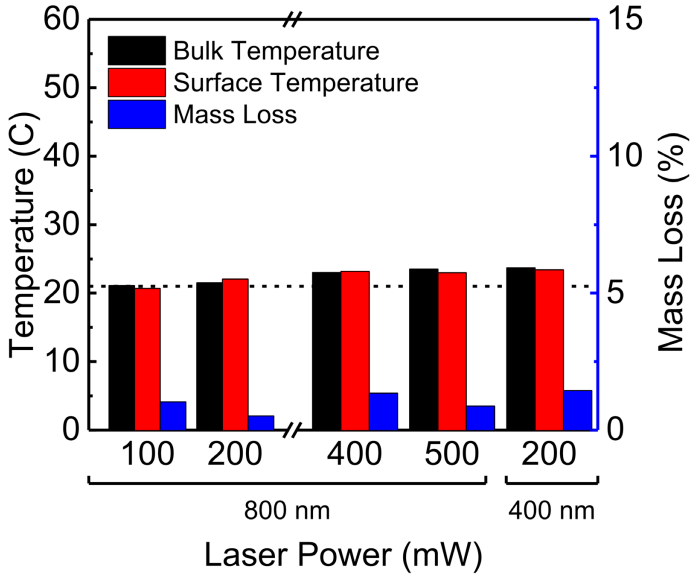

Figure S14. Photothermal heating of pure water without Al@SiO_2 NCs. The dashed line represents room temperature

REFRENCES

1. Clark, B. D.; Desantis, C. J.; Wu, G.; Renard, D.; McClain, M. J.; Bursi, L.; Tsai, A. L.; Nordlander, P.; Halas, N. J., Ligand-Dependent Colloidal Stability Controls the Growth of Aluminum Nanocrystals. *Journal of the American Chemical Society* **2019,** *141* (4), 1716-1724.
2. McClain, M. J.; Schlather, A. E.; Ringe, E.; King, N. S.; Liu, L.; Manjavacas, A.; Knight, M. W.; Kumar, I.; Whitmire, K. H.; Everitt, H. O.; Nordlander, P.; Halas, N. J., Aluminum Nanocrystals. *Nano letters* **2015,** *15* (4), 2751-2755.
3. Renard, D.; Tian, S.; Ahmadivand, A.; DeSantis, C. J.; Clark, B. D.; Nordlander, P.; Halas, N. J., Polydopamine-Stabilized Aluminum Nanocrystals: Aqueous Stability and Benzo[a]pyrene Detection. *ACS Nano* **2019,** *13* (3), 3117-3124.
4. Stöber, W.; Fink, A.; Bohn, E., Controlled growth of monodisperse silica spheres in the micron size range. *Journal of Colloid and Interface Science* **1968,** *26* (1), 62-69.
5. *Handbook of optical constants of solids*. Academic Press: Orlando, 1985.
6. Cheng, F.; Su, P. H.; Choi, J.; Gwo, S.; Li, X.; Shih, C. K., Epitaxial Growth of Atomically Smooth Aluminum on Silicon and Its Intrinsic Optical Properties. *ACS Nano* **2016,** *10* (11), 9852-9860.